I S A V

Journal of Theoretical and Applied Vibration and Acoustics

journal homepage: http://tava.isav.ir

Numerical solution of unsteady flow on airfoils with local membrane in transient and laminar flows

Alireza Naderi [a], **Mohammad Mojtahedpoor** [*,b]

[a] *Assistant Professor, Aerospace complex, Malek-Ashtar University of Technology, Tehran, Iran*

[b] *Ph.D. Candidate, Aerospace complex, Malek-Ashtar University of Technology, Tehran, Iran*

KEYWORDS

Article history:
Received 05 December 2015

Received in revised form 19 January 2016

Accepted 11 Feburary 2016

Available online 01 March 2016

Keywords:
Finite volume element

Fluid solid interaction

Local flexible membrane

Low Reynolds number

ABSTRACT

Unsteady flow separation on the airfoils with local flexible membrane (LFM) has been investigated in transient and laminar flows by the finite volume element method. A unique feature of the present method compared with the common computational fluid dynamic softwares, especially ANSYS CFX, is the modification using the physical influence scheme in convection fluxes at cell surfaces. In contrary to the common softwares which use mathematical methods for discretization, this method considers the physical effects on approximation and discretization and thus increases the accuracy of solution and decreases the diffusion errors significantly. We have focused on the effects of deformation of the membrane on aerodynamic characteristics. For this purpose, first, we have solved the flow on NACA0012 airfoil in Reynolds number of 5000 and investigated the effects of local flexible membrane on aerodynamic coefficients in laminar flow. Then, we have solved the flow over LH37 airfoil in Reynolds number of 1.1×106 and studied the effects of flexible membrane on aerodynamic characteristics in transient flow. To calculate the Reynolds stress in turbulence equations, transient $\gamma - Re_\theta$ model has been used. According to the results, airfoil with local flexible membrane prevents flow separation, eliminates laminar separation bubble (LSB) and delays the stall.

1. Introduction

Common airfoils can perform excellent lift and lift-drag ratio characteristics in a certain range for the angles of attack. However, the attached flow changes to separation at high angles of attack beyond the critical value, which would reduce the lift coefficient dramatically and then enters the stall state. In nature, flying creatures are able to adapt variable atmosphere conditions by wing's deformation which may catch and control the fluid around their wings. Researchers hope to apply the flexible materials to the adaptive deformation airfoils to broaden the range of operating angles of attack for the airfoils, inspired by the flying animals. However, the specific

* Corresponding Author: Mohammad Mojtahedpoor, Email: Mojtahedpoor@gmail.com

flow mechanisms are still unknown. Researchers have done a good deal of investigations in this field which focused on the active and passive control mainly. In terms of active control, Gabor [1] and Hasegawa [2] made a good aerodynamic performance of the flexible airfoil through controlling the motion law actively. Chuijie et al. [3] manufactured a "Fluid Roller Bearing" effect by giving a suitable traveling wave deformation on the upper surface of the airfoil actively, which hinders the boundary layer separation effectively. Curet et al. [4] presented that using the electrical excitation approach to control the vibration of the flexible wings can improve the lift coefficient in a specific frequency range significantly. On the other hand, in passive control, Lian et al. [5, 6] presented that the coupling interaction of the dynamic effects with the mean curvature of the membrane wing can improve the lift effectively especially at high angles of attack and delays the occurrence of stall [7]. Albertani et al. [8] and Radmanesh [9] showed that the distribution of flexible structure and materials flexibility have an important effect on the amplitude and frequency of the flexible wings. There is a coupling interaction between the vibration characteristics of flexible wings and the fluctuations of flow field parameters which is demonstrated by Rojratsirikul [10]. Shy [11] showed the airfoil still has a well aerodynamic stability in the case of pulsating inflow.

Flexible structures, such as shell, plate, shallow arch and membrane etc., have been used widely in the high-performance aircraft, especially in micro air vehicles [12, 13]. Many experiments and numerical researches have presented that the flexible airfoil, compared with the rigid one, can delay flow separation, increase lift and decrease drag efficiently [10, 14]. Flow separation can easily occur for laminar flow, at low Reynolds numbers and results in complex unsteady separated flow even the transition to turbulence. In such flow, small perturbation such as the oscillation of flexible structure, can change the flow structure and airfoil performance dramatically. Chimakurthi et al. [15] showed a computational aeroelasticity framework for the flapping wing micro air vehicles and investigated both rigid and flexible wings. Lee et al. [12] studied the two-dimension insect flapping wing, and showed that structural flexibility has a significant effect on aerodynamic performance. In addition, some important physical phenomena, such as vortex pairing and vortex staying, were observed. Kang et al. [16] introduced the local flexible structure to control the flow and improved the aerodynamic performance significantly. Compared with the fully flexible wing, it is easier to use local flexible structure to fulfill the requirements of active control plus it can be used in normal or large size airfoils. However, airfoil with flexible structure usually involves complex and complicated fluid-structure interaction giving rise to a wide range of phenomena related to the high aerodynamic performance. The unsteady flow separation, however, is generally the original source of many complex flow structures such as vortex formation, wake flow etc. Therefore, a deep understanding of the unsteady flow separation and related flow structure can lead to a way to explain many complicated and different phenomena in unsteady flow.

To calculate the Reynolds stress in turbulence equations we need to use a turbulence model. $SST\ k-\omega$ turbulence model, coupled with a two-equation $\gamma - Re_\theta$ transient model has been published in 2009 by Mentre [17, 18]. The basic idea of this model was based on the idea of Blumer and Driest [19]. According to their study, the vortex Reynolds number can be used as an interface between Reynolds number at the beginning of transition which is obtained from experimental values and local boundary layer values. Therefore, we do not need to integrate the velocity profile over the boundary layer to determine the beginning of the transition. Two

equations of γ and Re_θ do not model the flow physics and only enter a wide range of experimental coefficients into the formulation [17, 18].

This study has been divided to two parts. First, we have investigated laminar flow over NACA0012 airfoil with local flexible membrane (LFM) in Reynolds number of 5000. The material of the membrane is thermoset polyurethane. A unique feature of the present method as compared with the common computational fluid dynamic softwares, especially ANSYS CFX, is the modification by using the physical influence scheme in convection fluxes at cell surfaces. This method considers the physical effects on approximation and discretization in contrary to the common softwares which use mathematical methods for discretization and thus it increases the accuracy of solution and decreases diffusion errors significantly. To analyze the aeroelastic system, the equations have been solved by pressure-based algorithm in each time step. Then, the calculated force in each step will be applied to the membrane's surface and the displacement of the membrane will be obtained by the Galerkin method. We considered four different cases in laminar flow. Rigid airfoil, airfoil with LFM at 0-0.1, 0.1-0.5 and 0.5-0.8 chord lengths. By solving the flow over the mentioned airfoils, the effect of LFM will be obtained.

Second, we have investigated the effect of LFM over LH37 airfoil in transient flow. The location of flexible membrane and Reynolds number are set to 0.2-0.7 chord length and 1.1×106 respectively. We considered aluminum as the membrane. To calculate the Reynolds stress we have considered $\gamma - Re_\theta$ transient model.

2. Numerical method

The governing equation in fluid phase includes the conservation of mass and momentum that in the Lagrangian space will be written as follows:

$$\frac{d}{dt}\iint_{\vartheta(t)} \rho d\vartheta + \iiint_{S(t)} \rho\left(\vec{V} - \vec{V}'\right).dS = 0$$
$$\frac{d}{dt}\iint_{\vartheta(t)} \rho\vec{V} d\vartheta + \iiint_{S(t)} \rho\vec{V}\left(\vec{V} - \vec{V}'\right).dS = \iint_{S(t)} \sigma\hat{n}dS \quad (1)$$

where $V = u\hat{\imath} + v\hat{\jmath}$ is the fluid velocity vector, $\acute{V} = \acute{u}\hat{\imath} + \acute{v}\hat{\jmath}$ is the velocity vector of finite volume surfaces, $dS = (dS_x)\hat{\imath} + (dS_y)\hat{\jmath}$ is the normal vector with magnitude of $dS = [(dS_x)^2 + (dS_y)^2]^{1/2}$, □ is the volume of each finite volume, ρ is density of fluid and σ is total strain tensor.

In this study, we have used the Lagrangian-Eulerian approach to solve the fluid flow field by the finite volume element method [20, 21]. The approximation of time is second order. To approximate diffusion terms we have used shape functions of finite element method. The pressure terms will be approximated by shape functions. The convection terms will be approximated by the upwinding method and using physical influences. Complex domains have been solved by this method and the results showed that the current method is able to calculate fluxes in triangular and quadrilateral elements exactly [20, 21].

Moving boundaries are excited by the fluid flow for coupling of the fluid and the structure. To extract the structure governing equations, moving boundaries were considered as a beam. The thickness of the beam is h and the length is L. For a fixed beam with length L, thickness of h and

unit width ($b = 1$), the moment of inertia is $I = \frac{1}{12}h^3$. We have used two-dimensional finite volume element methods to solve find the displacement of the beam.

$$EI\frac{\partial w}{\partial x^2} + \zeta A\frac{\partial^2 w}{\partial t^2} = f\left(x,t\right) \tag{2}$$

where w is the displacement of the beam, E is the modulus of elasticity, ζ is the density of the membrane, A is the cross section of the membrane and $f(x,t)$ is the time-dependent load distribution. Finally, after simplification, the displacement of the membrane will be obtained as follows:

$$w\left(x\right) = N_1 w_1 + N_2\frac{dw_1}{dx} + N_3 w_3 + N_4\frac{dw_2}{dx} \tag{3}$$

where N_1, N_2, N_3 and N_4 are the shape functions in the finite element method. After assembling, the matrix equation is achieved:

$$\left\{\left[M\right] - \lambda_n\left[K\right]\right\}\left\{Q\right\} = F \tag{4}$$

where F is the force vector, Q is the nodes' displacement vectors, [M] is the total mass of the elements, [K] is the stiffness matrix and λ_n is the eigenvalues vectors. Equation 4 formulates the displacement of the membrane. The grid is unstructured. Figures 1.a and 1.b show the computational grid. We have used quadrilateral elements on the surrounding of the airfoil and a little farther up to free boundaries, we have used unstructured triangular elements. The distance of the center of the airfoil up to free boundaries is 14. Inlet velocity at inlet boundary and the value of pressure at outlet boundary is unit. In order to evaluate the sensitivity of computational domain to grids, we have considered three different grids with node numbers of 9000, 14000 and 28000 respectively in Reynolds number of 5000 and angle of attack of 6 degrees. Figure 2 shows grid sensitivity and the results show little differences in different grids. According to Fig. 2 the fine and medium grids are coincided. In all cases, we have used computational domain with node number of 14000 and time step of 0.01 s.

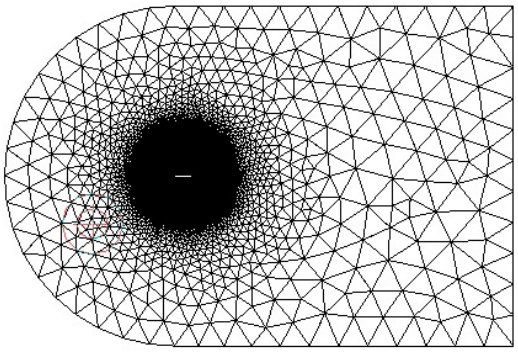

Fig. 1. (a) Computational domain

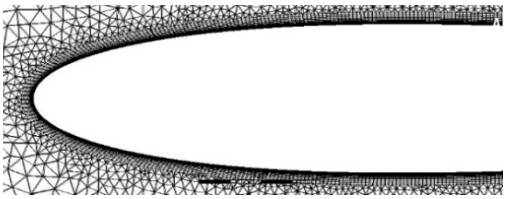

Fig. 1. (b) Computational domain in details

3. Laminar flow

In this section by using the LFM in different locations, we have investigated the effect of LFM on aerodynamic characteristics in laminar flow. The material of membrane is chosen thermoset polyurethane. First, the location of the membrane is set to 0-0.1 chord length, and then by changing the location of the membrane to 0.1-0.5 and 0.5-0.8 cord lengths, the effect of these variations has been studied. The physical properties of membrane have been shown in Table 1.

Table 1. Physical properties of thermoset polyurethane

Property	**Unit**	**Value**
Density	kg/m^3	5850
Module of elasticity	Pa	8×10^4
Thickness of membrane	m	10^{-3}

3.1. Results validation

To verify the results, we have compared our results with Lei et al. [22] which has been done in 2014. In accordance with their study, NACA0012 airfoil with LFM is chosen as an example. In particular, the Reynolds number is set to 5000. The LFM is located at 0−0.1 chord length of airfoil as shown in Fig. 3.

The time-averaged drag coefficients of the airfoil with LFM at various angles of attack are compared with Lei et al. [22] as shown in Fig. 4. According to Fig. 4, the drag coefficients at different angles of attack agree well with the results of Lei et al. [22].

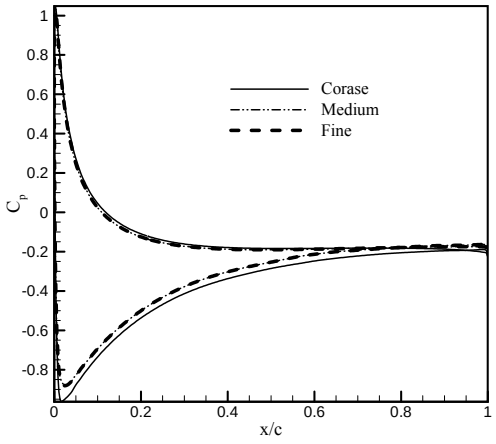

Fig. 2. Grid study

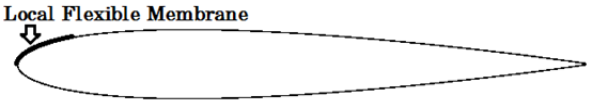

Fig. 3. Location of local flexible structure on NACA0012 airfoil

3.2. LFM at 0-0.1 chord length

Effects of LFM at 0-0.1 chord length on aerodynamic characteristics at Reynolds number of 5000 have been illustrated in Fig. 5. According to Fig. 5, at low angles of attack, the LFM has a little effect on the lift and drag coefficients compared with rigid airfoil. By changing the AOA from 5 degrees to higher angles, lift coefficient in airfoil with LFM has increased sharply. While the drag coefficient is almost the same as the rigid one. It is clear that the rapid changing of lift is consistent with the sudden jump of the oscillation amplitude. Figure 6 shows the time-averaged pressure on rigid airfoil and airfoil with LFM. As it is obvious, the time-averaged pressure on the upper surface of airfoil with LFM is much lower than rigid airfoil at angle of attack of 8 degrees. Figure 7 shows streamlines on airfoil with LFM and rigid airfoil at AOA=8o. According to Fig. 7, using LFM makes large separation bubble, prevents sudden separation, and improves aerodynamic characteristics.

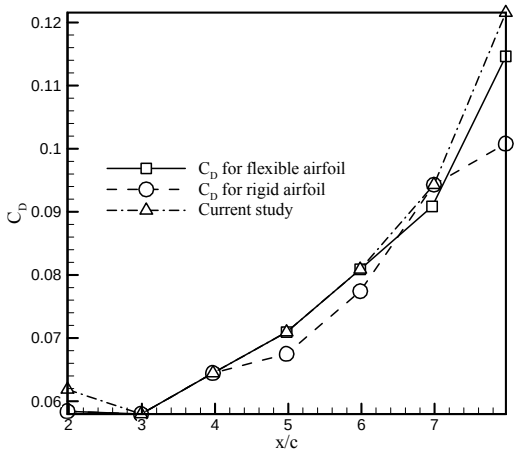

Fig. 4. Results validation for airfoil with flexible membrane at Re=5000

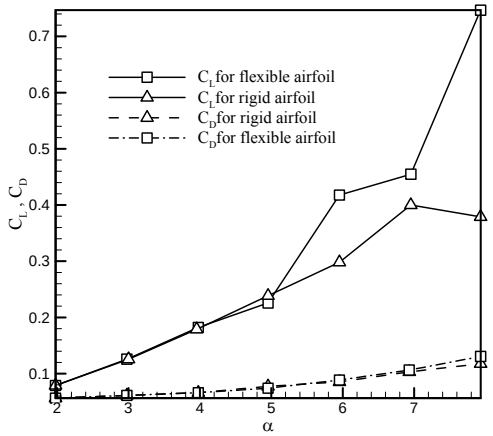

Fig. 5. Lift coefficient in airfoil with local flexible membrane at 0-0.1 chord length and Re=5000

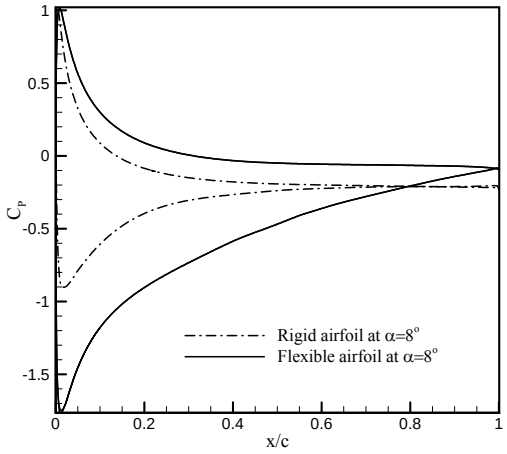

Fig. 6. Pressure comparison between rigid airfoil and airfoil with LFM

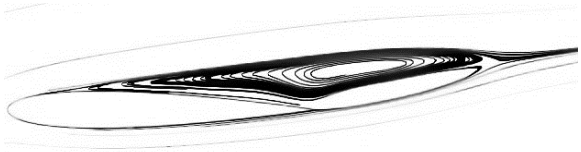

Fig. 7. (a) Streamlines on rigid airfoil at AOA of 8°, Re=5000

Fig. 7. (b) Streamlines on flexible airfoil at AOA of 8°, Re=5000

3.3. LFM at 0.1-0.5 chord length

In this section, we have investigated the effects of LFM at 0.1-0.5 chord length and at Reynolds number of 5000. Figure 8 shows lift coefficients on this airfoil. According to Fig. 8, at low angles of attack, the lift coefficients have increased gradually than airfoil with LFM at 0-0.1 chord length. However, by increasing the AOA this benefit has been reduced and finally at AOA=8°, the lift coefficient than airfoil with LFM at 0-0.1 chord length has decreased. We should note that according to Fig 9, drag coefficient in this case than rigid airfoil and LFM at 0.1-0.5 chord length is lower relatively. Pressure coefficients at different angles of attack have been shown in Fig. 10.

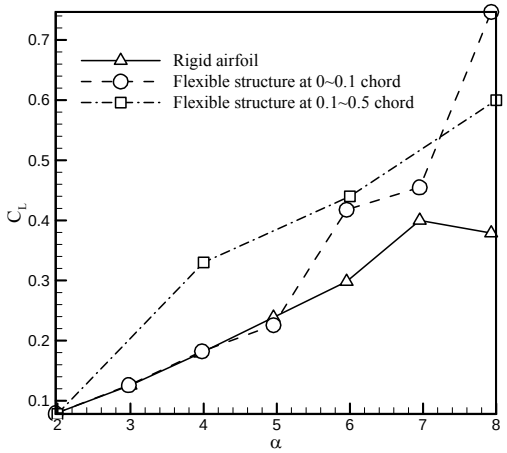

Fig. 8. Lift coefficients comparison in different LFM

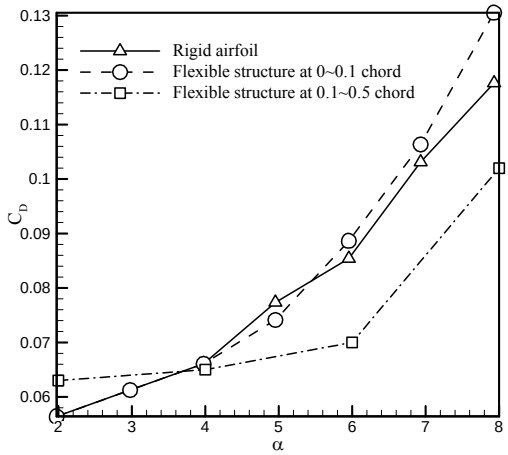

Fig. 9. Drag coefficients comparison in different LFM

3.4. LFM at 0.5-0.8 chord length

In this part, we have placed the LFM at 0.5-0.8 chord length. Figures 11 and 12 show lift and drag coefficients on rigid airfoil and LFM airfoils respectively. In accordance with Fig. 11, by changing the LFM location from 0.1-0.5 chord length to 0.5-0.8 chord length, we do not meet significant changes. At angle of attack of 2 degrees, due to attachment of boundary layer the lift coefficient is almost constant in all LFM locations. However, by increasing of angle of attack and separation phenomena, the LFM makes LSB, prevents separation and increases lift coefficient. Although the maximum amount of lift coefficient appears at angle of attack of 8 degrees and LFM location of 0-0.1 chord length.

According to Fig. 12, drag coefficient in airfoil with LFM does not meet significant changes than rigid airfoil. This parameter shows the desirable effect of airfoil with LFM. However, the minimum amount of drag coefficient appears at LFM locations of 0-0.5 and 0.5-0.8 chord length.

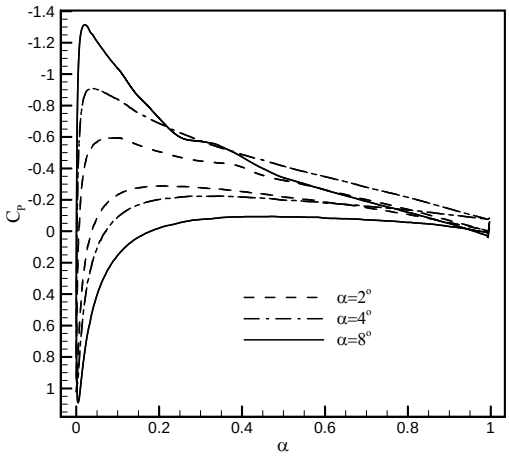

Fig. 10. Pressure coefficients over flexible airfoils in different angles of attack

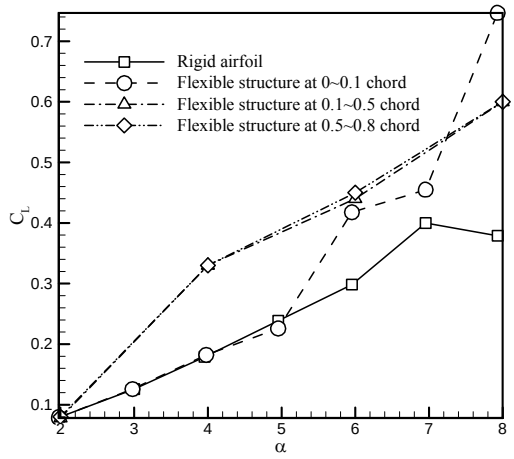

Fig. 11. Lift coefficients comparison in different angles of attack

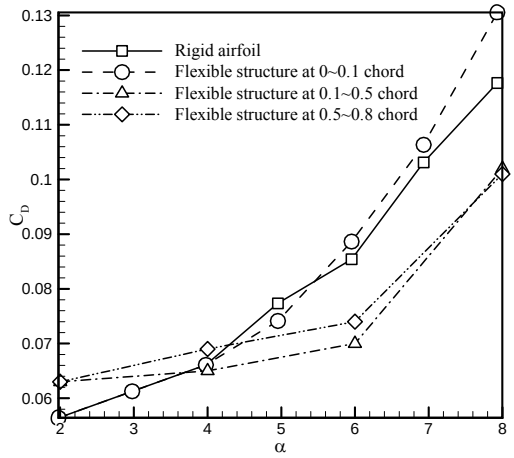

Fig. 12. Drag coefficients comparison in different angles of attack

Figure 13 shows pressure coefficients at angle of attack of 8 degrees, Re=5000 and different LFM locations. As we expect, the maximum area under the curve belongs to airfoil with LFM at location of 0-0.1 chord length which has the maximum of lift coefficient as well.

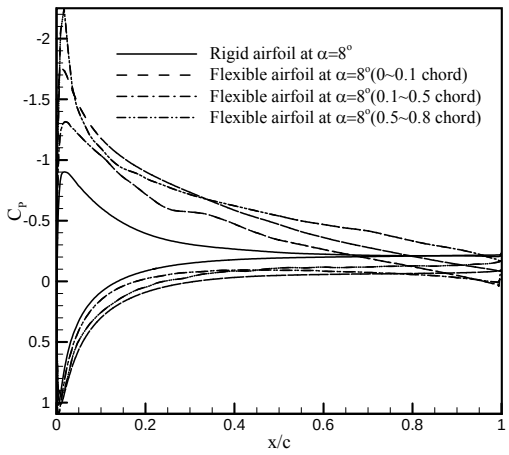

Fig. 13. Pressure coefficients at different membrane location, AOA=8 degrees, Re=5000

4. Transient flow

In this section, we have solved the fluid flow over LH37 airfoil in Reynolds number of 1.1×106. The material of membrane is chosen aluminum alloy. LH37 airfoil has been designed for range of Reynolds number of 106 and the airfoil presents high lift coefficients relatively. Flow separation occurs in this range and the flow reattaches to the airfoil surface because of high momentum of turbulence and makes LSB [23]. Maximum thickness of LH37 is 17.5 percent and located at x/c=0.354. Maximum chamber line is 0.04 and located at x/c=0.385. LH37 presents low drag coefficients for lift coefficient range of 0.3 up to 1.5 [24]. Therefore, we have located the membrane at 0.2-0.7 chord length and investigated the effect of LFM on aerodynamic parameters in transient flow. Physical properties of aluminum alloy membrane have been shown in Table 2.

Table 2. Physical properties of aluminum alloy

Property	Unit	Value
Density	kg/m^3	2550
Module of elasticity	Pa	5×10^7
Thickness of membrane	m	10^{-3}

4.1. Results validation

To validate our results in transient flow, we have compared our results with the experiments done by Schaw et al. [24]. Figure 14 shows lift coefficient comparison between our results and Schawe's results on rigid airfoil at Reynolds number of 1.1×106 and different angles of attack. According to Fig. 14, the desired accuracy of present study compared with experimental results is obvious.

4.2. LFM at 0.2-0.7 chord length

In this section, by using of LFM at 0.2-0.7 chord length of LH37 airfoil, we have studied the effect of LFM on aerodynamic parameters in transient flow. LH37 airfoil configuration and the location of membrane have been shown in Fig. 15. Lift coefficient comparison graphs between rigid airfoil and LFM have been illustrated in Fig. 16. According to Fig. 16, using LFM did not have significant improvement on lift coefficient until the creation of LSB (AOA=8^o). However, LFM eliminates LSB on upper surface of the airfoil and increases the lift coefficient after creation of bubble. The LFM increases lift coefficient significantly and delays the stall phenomena. The location of LSB on lower surface of airfoil with LFM has been shown in Fig. 17. According to Fig. 17, LFM removes LSB from upper surface of airfoil.

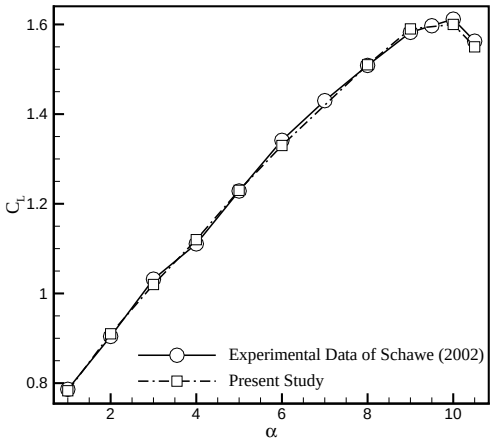

Fig. 14. Validation of results in transient flow

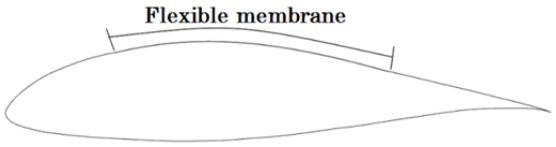

Fig. 15. LH37 airfoil configuration

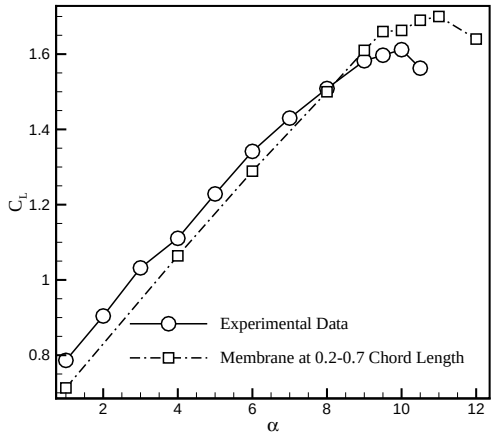

Fig. 16. Lift coefficient comparison on rigid and flexible LH37 airfoil

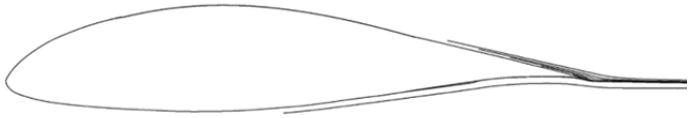

Fig. 17. (a) Streamlines on flexible LH37 airfoil – Re=1.1×10^6

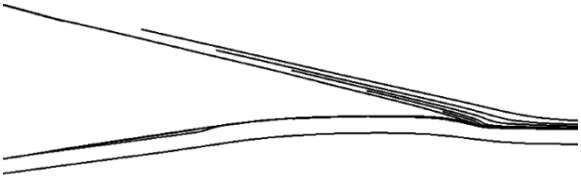

Fig. 17. (b) Streamlines on flexible LH37 airfoil – Re=1.1×10^6 – Close up view

Figure 18 shows a comparison between rigid airfoil and airfoil with LFM in transient flow. According to Fig. 18, significant effect of LFM on improvement of drag coefficient is obvious. The membrane by eliminating the LSB and separation prevention, decreases the drag coefficient significantly. For better understanding, Fig. 19 compares lift to drag coefficients and shows optimal performance of airfoil with LFM in transient flow.

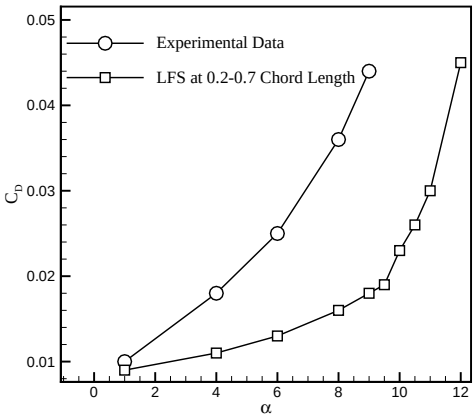

Fig. 18. Drag coefficient comparison on flexible and rigid LH37 airfoil

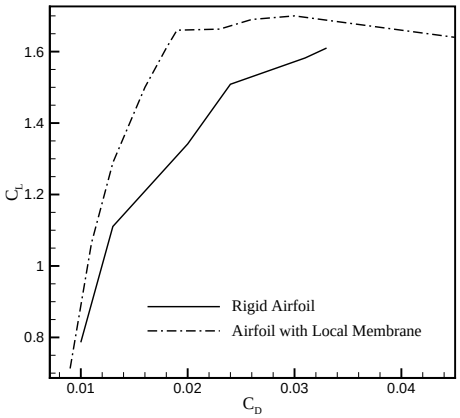

Fig. 19. CL to CD comparison graph on flexible and rigid LH37 airfoil

5. Conclusion

In this study, we have investigated the effect of LFM on aerodynamic characteristics numerically in laminar and transient flows by finite volume element method. A unique feature of present method than common computational fluid dynamic software, especially ANSYS CFX is the modification by using of physical influence scheme in convection fluxes at cell surfaces. This method by considering physical effects on approximation and discretization contrary to the common software that use mathematical methods for discretization, increases the accuracy of solution and decreases diffusion errors significantly. To solve the Reynolds stress in turbulence equations, we used $\gamma - Re_\theta$ transient model.

In laminar flow, we chose membrane with material of thermoset polyurethane on NACA0012. The Reynolds number is set to 5000. To investigate the effect of location of LFM on aerodynamic characteristics, we located the membrane at 0-0.1, 0.1-0.5 and 0.5-0.8 chord lengths respectively. According to the results, by using of LFM especially at high angles of attack which flow separation happens, LFM makes LSB, prevents the flow separation and increases the lift coefficient. The airfoil met the maximum lift coefficient at angle of attack of 8 degrees and membrane location of 0-0.1 chord length. The results show, LFM does not have a significant effect on drag coefficient and airfoil met minimum value of drag at membrane locations of 0.1-0.5 and 0.5-0.8 chord length.

In transient flow, we used LFM on LH37 airfoil and membrane location of 0.2-0.27 chord length. The Reynolds number is set to 1.1×10^6. According to the results, LFM eliminates LSB from upper surface of airfoil and improves airfoil performance. The stall angle has been delayed from 10.5 to 12 angles as well.

References

[1] O.S. Gabor, A. Koreanschi, R.M. Botez, Low-speed aerodynamic characteristics improvement of ATR 42 airfoil using a morphing wing approach, in: IECON 2012-38th Annual Conference on IEEE Industrial Electronics Society, IEEE, 2012, pp. 5451-5456.
[2] H. Hasegawa, S. Kumagai, Adaptive separation control system using vortex generator jets for time-varying flow, Journal of applied fluid mechanics, 1 (2008) 9-16.
[3] W. Chuijie, X. Yanqiong, W. Jiezhi, "Fluid roller bearing" effect and flow control, Acta Mechanica Sinica, 19 (2003) 476-484.
[4] O.M. Curet, A. Carrere, R. Waldman, K.S. Breuer, Aerodynamic characterization of wing membrane with adaptive compliance, in: 54th AIAA/ASME/ASCE/AHS/ASC Structures, Structural Dynamics, and Materials Conference, 2013, pp. 1909.
[5] Y. Lian, W. Shyy, Three-dimensional fluid-structure interactions of a membrane wing for micro air vehicle applications, AIAA Paper, 1726 (2003) 2003.
[6] Y. Lian, W. Shyy, D. Viieru, B. Zhang, Membrane wing aerodynamics for micro air vehicles, Progress in Aerospace Sciences, 39 (2003) 425-465.
[7] R.E. Gordnier, High fidelity computational simulation of a membrane wing airfoil, Journal of Fluids and Structures, 25 (2009) 897-917.
[8] R. Albertani, B. Stanford, J.P. Hubner, P.G. Ifju, Aerodynamic coefficients and deformation measurements on flexible micro air vehicle wings, Experimental Mechanics, 47 (2007) 625-635.

[9] M. Radmanesh, O. Nematollahi, M. Nili-Ahmadabadi, M. Hassanalian, A novel strategy for designing and manufacturing a fixed wing MAV for the purpose of increasing maneuverability and stability in longitudinal axis, Journal of Applied Fluid Mechanics, 7 (2014) 435-446.
[10] P. Rojratsirikul, Z. Wang, I. Gursul, Unsteady fluid–structure interactions of membrane airfoils at low Reynolds numbers, Experiments in Fluids, 46 (2009) 859-872.
[11] W. Shyy, F. Klevebring, M. Nilsson, J. Sloan, B. Carroll, C. Fuentes, Rigid and flexible low Reynolds number airfoils, Journal of Aircraft, 36 (1999) 523-529.
[12] K.B. Lee, J.H. Kim, C. Kim, Aerodynamic effects of structural flexibility in two-dimensional insect flapping flight, Journal of aircraft, 48 (2011) 894-909.
[13] A. Saboonchi, S. Hassanpour, Heat transfer analysis of hot-rolled coils in multi-stack storing, Journal of materials processing technology, 182 (2007) 101-106.
[14] N.J. Pern, J.D. Jacob, Wake vortex mitigation using adaptive airfoils - The piezoelectric arc airfoil, in: AIAA, Aerospace Sciences Meeting and Exhibit, 37 th, Reno, NV, 1999.
[15] S.K. Chimakurthi, J. Tang, R. Palacios, C.E. S. Cesnik, W. Shyy, Computational aeroelasticity framework for analyzing flapping wing micro air vehicles, AIAA journal, 47 (2009) 1865-1878.
[16] W. Kang, J.Z. Zhang, P.H. Feng, Aerodynamic analysis of a localized flexible airfoil at low Reynolds numbers, Communications in Computational Physics, 11 (2012) 1300-1310.
[17] R.B. Langtry, J. Gola, F.R. Menter, Predicting 2D airfoil and 3D wind turbine rotor performance using a transition model for general CFD codes, AIAA paper, 395 (2006) 2006.
[18] R.B. Langtry, F.R. Menter, Correlation-based transition modeling for unstructured parallelized computational fluid dynamics codes, AIAA journal, 47 (2009) 2894-2906.
[19] C.B. Blumer, E.R. van Driest, Boundary layer transition-freestream turbulence and pressure gradient effects, AIAA Journal, 1 (1963) 1303-1306.
[20] M. Darbandi, M. Taeibi-Rahni, A. Reza Naderi, Firm structure of the separated turbulent shear layer behind modified backward-facing step geometries, International Journal of Numerical Methods for Heat & Fluid Flow, 16 (2006) 803-826.
[21] A. Naderi, M. Darbandi, M. Taeibi-Rahni, Developing a unified FVE-ALE approach to solve unsteady fluid flow with moving boundaries, International journal for numerical methods in fluids, 63 (2010) 40-68.
[22] P.F. Lei, J.Z. Zhang, W. Kang, S. Ren, L. Wang, Unsteady flow separation and high performance of airfoil with local flexible structure at low Reynolds number, Communications in Computational Physics, 16 (2014) 699-717.
[23] G. Wichmann, C.H. Rohardt, P. Hirt, Kenndaten für Profile: Profil DLRLH37, in, Luftfahrttechnisches Handbuch – LTH, Band Aerodynamik AD 41102-24, 1998.
[24] D. Schawe, C.H. Rohardt, G. Wichmann, Aerodynamic design assessment of Strato 2C and its potential for unmanned high altitude airborne platforms, Aerospace science and technology, 6 (2002) 43-51.